Available online at www.sciencedirect.com

SCIENCE DIRECT®

Journal of Marine Systems 50 (2004) 199–222

JOURNAL OF MARINE SYSTEMS

www.elsevier.com/locate/jmarsys

A plankton population model with biomechanical descriptions of biological processes in an idealised 2D ocean basin

Mark E. Baird[a,*], Peter R. Oke[a], Iain M. Suthers[b], Jason H. Middleton[a]

[a] *School of Mathematics, University of NSW, Sydney NSW 2052, Australia*
[b] *School of Biological, Earth and Environmental Sciences, University of NSW, Sydney NSW 2052, Australia*

Received 14 March 2003; accepted 27 February 2004
Available online 30 April 2004

Abstract

A five component pelagic ecosystem model is coupled to a two dimensional configuration of the Princeton Ocean Model (POM), representing an idealised ocean basin with upwelling and downwelling regions. The formulation of the biological equations is based on biomechanical descriptions of the processes of nutrient uptake, light capture, sinking and predator–prey encounter rates. The biological equations have mathematical similarities to existing process-based models which use empirical descriptions of biological processes. These similarities are exploited to determine the planktonic sizes which best correspond to the microzooplankton parameter set in the Edwards et al. (J. Plankton Res. 22 (2000) 1619) modelling study that uses the Franks et al. NPZ model (Mar. Biol. 91 (1986) 121). Simulations show the biomechanical model produces a deep chlorophyll maximum (DCM) when a stable surface mixed layer is present, and a surface bloom during wind-driven coastal upwelling. The Franks biological model is coupled to the physical configuration used for the biomechanical model, and the output from the two models compared in the coastal upwelling region. The behaviour of the biomechanical model is further investigated by undertaking supplementary simulations with the biological parameter values determined (1) using size-based relationships only, (2) using size-based relationships without sinking of phytoplankton and zooplankton, (3) by doubling the cell radii. These simulations provide a preliminary assessment of the biomechanical, size-based approach, and shed light on physical processes at the scale of individual planktonic cells that are determining the rates of biological processes.

Keywords: Plankton; Size; Upwelling; Deep chlorophyll maximum; Princeton Ocean Model; East Australian Current

1. Introduction

Pelagic ecosystems consist of planktonic organisms with a range of sizes (Sheldon et al., 1972). The size of plankton cells affects the rate of many biological processes such as nutrient uptake and planktonic growth (Reynolds, 1984). The interaction of size-dependent planktonic processes with environmental factors such as nutrient concentration, light, turbulence and temperature determines to a large extent the assemblage of organisms that dominate an environment (Kiørboe, 1993).

Size-dependent planktonic processes include nutrient uptake (Hein et al., 1995), light capture (Finkel and Irwin, 2000), growth (Gillooly, 2000), respiration

* Corresponding author. Tel.: +61-293857196; fax: +61-293857123.
E-mail address: mbaird@maths.unsw.edu.au (M.E. Baird).

0924-7963/$ - see front matter © 2004 Elsevier B.V. All rights reserved.
doi:10.1016/j.jmarsys.2004.02.002

(Tang and Peters, 1995), grazing selection (Caparroy et al., 2000), grazing rates (Hansen et al., 1997), sinking (Kiørboe, 1993), and swimming (Sommer, 1988). Furthermore, properties of plankton cells such as density and elemental content are known to be size-dependent (Strathmann, 1967). Ideally, models of planktonic communities should be formulated in such a way to take advantage of these documented size dependencies.

One such example, developed for plankton communities in lakes, is the Phytoplankton Response to Environmental Change (PROTECH) model (Elliott et al., 2000). PROTECH represents phytoplankton properties and processes as a function of the size and surface area to volume ratio, as obtained from experimental data. PROTECH illustrates that much of the observed plankton population dynamics can be accounted for by using empirical size-based relationships. The choice of the surface area to volume ratio also represents an additional understanding of a physical process affecting nutrient uptake beyond empirical size-based observations (Reynolds, 1989).

Baird and Emsley (1999) and Emsley (2000) took a more theoretical approach to incorporating size-based relationships in a pelagic ecosystem model. The biological interactions were quantified by using an assumption that planktonic processes were limited by geometrically dependent physical processes. Under this assumption, it is possible to approximate the rates of a number of the planktonic processes using a cell radius only. For example, Baird and Emsley (1999) approximated grazing rates of zooplankton on phytoplankton at low phytoplankton concentrations by the rate of encounter of spheres of the size of the phytoplankton and zooplankton cells. Such approximations do not affect the complexity of the planktonic ecosystem model which is still determined by the number of state variables, but rather provide an alternative, geometric methodology for formulating the biological model and determining parameter values that are used to quantify the rates of planktonic interactions.

The potential benefits of using biomechanical descriptions are both theoretical and practical. Biomechanical descriptions relate more directly to environment variables such as temperature and small-scale turbulence intensity, and more clearly show how far our understanding of the biomechanical planktonic processes can replicate observed plankton dynamics. Practically, biomechanical descriptions are often related to only a few physically meaningful parameters, in particular plankton radii. As a result, the number of parameters required to implement such a model is significantly decreased.

This paper couples a simplified version of the Baird and Emsley (1999) plankton population model to a two-dimensional configuration of the Princeton Ocean Model (POM). The continental shelf profile of the configuration is representative of a cross-shelf slice of the East Australian Continental Shelf off Diamond Head, NSW (31°44′ S). The model is spun-up using a sinusoidally varying wind stress to produce a stable surface mixed layer. A constant, long duration wind stress is then applied. The changing biological fields represent the response to an upwelling favourable wind after a period of relative stability.

In the biomechanical model, phytoplankton and zooplankton cell radius determine the parameters affecting phytoplankton nutrient uptake, light absorption and sinking rates, and the encounter rates between zooplankton and phytoplankton cells. As a methodology for determining appropriate cell sizes to represent a pelagic ecosystem, and in order to facilitate a model intercomparison exercise, mathematical similarities between the biomechanical model and a popular NPZ model (Franks et al., 1986) with empirical descriptions are utilised. The Franks model was chosen because (1) it is a widely used model of plankton population dynamics (Edwards et al., 2000a; Franks and Chen, 2000; Spitz et al., 2003); (2) it contains empirical descriptions of biological processes with which the biomechanical model can be compared; (3) the Franks model includes the processes of light capture, nutrient uptake, grazing and sinking that are most easily represented by biomechanical relationships, and contains few processes that are difficult to represent biomechanically (such as detrital breakdown) and; (4) while superficially the Franks model and the presented biomechanical model have mathematical similarities (see Appendix C), the biological responses have interesting differences. The biomechanical model parameters determined by comparison with the Franks model are used in the main simulation presented in this paper, which is assessed against the output of the Franks model itself.

To further investigate the behaviour of the biomechanical model, supplementary simulations are run with parameter sets determined using:

(1) size-based relationships only, illustrating the behaviour of the biomechanical model when using primarily laboratory-determined parameters;
(2) as for (1) but with zero sinking velocities, investigating the effect of plankton maintaining their vertical position in the water column and;
(3) as for (2), but with double the cell radii, investigating the sensitivity of the biomechanical model to changes in plankton radii.

The aim of this paper is to introduce a coupled physical biomechanical pelagic ecosystem model, and to investigate its behaviour during an extended period with a stable surface mixed layer and during a 20-day wind driven upwelling event. Results are presented in terms of biological fields, and the rate of change of biological fields due to individual processes. The development of a deep chlorophyll (or phytoplankton) maximum (DCM) under a stable surface mixed layer, and a near-shore phytoplankton bloom due to coastal upwelling is analysed. The model behaviour is further explored by comparison to an existing NPZ model, and using three variations of the biological parameter set.

2. The physical model

The physical model is a configuration of the Princeton Ocean Model (POM) which solves the nonlinear primitive equations on sigma coordinates using finite difference methods (Blumberg and Mellor, 1987). The POM has a free surface and uses a split time step to solve the barotropic variables with greater temporal resolution than the baroclinic variables. The velocity **v** has components (u, v, ω) corresponding to the cross-shelf, alongshore and vertical velocities in the (x, y, σ) directions, so that u is positive offshore, v is positive towards the north and ω is positive upwards (normal to sigma surfaces). The vertical viscosity and diffusion coefficients are flow-dependent according to the level 2.5 turbulence sub-model of Mellor and Yamada (1982) with wave-enhanced mixing near the surface (Craig and Banner, 1994). Horizontal mixing is simulated using the Smagorinsky (1963) scheme. Details of the numerical techniques and method of solution are given by Blumberg and Mellor (1987).

The encounter rate of predators and prey in the biomechanical model is a function of the rate of dissipation of turbulent kinetic energy (TKE), ϵ, which can be derived from the level 2.5 turbulence scheme of Mellor and Yamada (1982). The POM has two state variables which represent turbulence: twice the turbulent kinetic energy per unit mass, q^2, and q^2 multiplied by a turbulence length scale, l. From these two state variables, ϵ can be calculated for the interior sigma layers from (Wijesekera et al., 2003):

$$\epsilon = \frac{q^3}{B_1 l} \tag{1}$$

where $B_1 = 16.6$ is an empirical constant (Blumberg and Mellor, 1987). The dissipation rate of TKE in the surface and bottom layers is given by:

$$\epsilon = \frac{u_*^3}{\kappa z_0} \tag{2}$$

where u_* is the friction velocity at the boundary, and is the square root of the shear stress per unit mass, κ is the von Kármán constant (~ 0.4) and the roughness length scale, $z_0 = 0.1$ m (Craig and Banner, 1994).

The physical model is configured to represent an idealised two-dimensional wind-driven circulation with no variations in the alongshore direction, and is similar to other two-dimensional physical studies (Allen et al., 1995; Edwards et al., 2000a). The idealised bathymetry is representative of a cross-shelf transect at Diamond Head, NSW (31°44′ S), on the east Australian coast, and a region known for upwelling (Rochford, 1972; Roughan and Middleton, 2002). The Coriolis parameter, f, at this latitude is $-7.07 \times 10^{-5}\ \mathrm{s}^{-1}$. The model grid contains 301 points in the x-direction, with a maximum horizontal grid spacing of 0.5 km, and 41 vertical sigma levels (Fig. 1). A log profile in the sigma levels is used to create greater resolution in the surface and bottom boundary layers. For further details of the grid configuration, see Appendix A. The barotropic variables are solved every 2 s, and the baroclinic variables every minute.

The alongshore boundary conditions are periodic for all variables in order to ensure uniformity in the

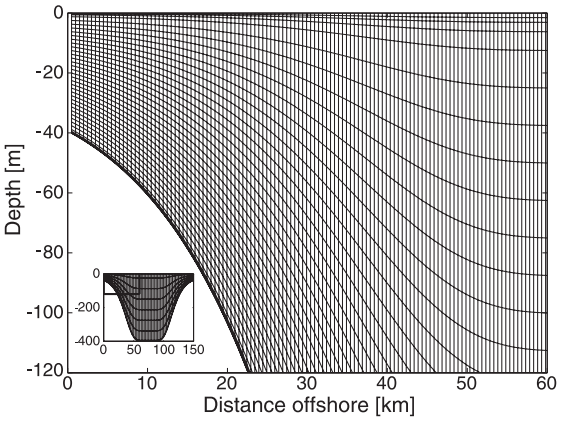

Fig. 1. The model grid. The full model domain is drawn in the insert with every fifth line drawn. The main figure shows the boxed western surface section of the model domain with every grid line drawn. Figs. 2–12 give model results from the boxed region.

alongshore direction. The boundary conditions at the coast include zero normal velocity, free slip tangential velocity and zero gradient for vertical velocity, temperature, T, salinity, S, and the variables related to the turbulence sub-model. The surface heat and freshwater fluxes are set to zero and the initial velocity field is at rest. The initial T and S fields are horizontally uniform, with the vertical profile interpolated from the annual average of the CSIRO Atlas of Regional Seas (Ridgway et al., 2002) at 30°S 153.5°E.

Unlike the studies of Allen et al. (1995) and Edwards et al. (2000a), the physical model is run for an extended period (375 days) before the constant upwelling-favourable winds are applied. This extended spin-up allows the biological state variables to reach a quasi steady state. The biological model is forced with incident photosynthetic available radiation (PAR), a function of the day of the year. The coupled biological-physical model simulation begins on Day -375, corresponding to October 21 in the austral spring. The constant upwelling-favourable winds are applied from Day 0 onwards, corresponding to November 1 of the following year. During the 375-day spin-up, 125 cycles of a 3-day period sinusoidal wind stress are completed, varying between 0.05 and -0.05 N m^{-2}. A wind stress of 0.05 N m^{-2} corresponds to a southerly wind of approximately 2.8 m s^{-1}. During the spin-up, T and S are nudged back to initial conditions on a time scale of 20 days to obtain a relatively constant surface mixed layer depth before the constant winds are applied.

On model Day 0, after the 375-day spin-up, T and S relaxation is removed. The sinusoidal wind stress was continued for another 1/4 cycle (or 3/4 of a day), to allow the alongshore wind stress to smoothly reach the maximum in the northerly direction of 0.05 N m^{-2}. After Day 0.75, the alongshore wind stress is maintained at a constant -0.05 N m^{-2}. The output of the model from Day 0 represents the response of a stable surface mixed layer to the onset of a constant alongshore wind stress.

3. The biological model with biomechanical descriptions

The biological model structure is a simple NPZ (nutrient/phytoplankton/zooplankton) model with additional state variables for the energy and nitrogen reserves of phytoplankton. The biological model is based on biomechanical descriptions of nutrient uptake, light capture, sinking and predator–prey encounter rates, which are similar to those in Baird and Emsley (1999) and Baird et al. (2003). Mortality is represented by commonly used exponential decay equations with empirical coefficients. A further analysis of the phytoplankton growth model has been undertaken in Baird et al. (2001).

3.1. Model equations

The biological model contains five state variables: dissolved inorganic nitrogen (DIN), N [mol N m^{-3}], phytoplankton nitrogen, P [mol N m^{-3}], zooplankton nitrogen, Z [mol N m^{-3}], phytoplankton energy reserves, R_I [mol photon cell^{-1}], and phytoplankton nitrogen reserves, R_N [mol N cell^{-1}]. For comparison, a commonly used alternate term for quantifying nitrogen reserves is total algal nitrogen or the cell quota, Q_N [mol N cell^{-1}], which is given by $Q_N = m_{P,N} + R_N$, where $m_{P,N}$ is the stoichiometry coefficient of nitrogen in phytoplankton, and represents the minimum quantity of nitrogen for which a cell remains viable. The parameter $m_{P,N}$ is obtained from a size-based relationship for C per cell (Table 1) and the Redfield ratio (C/N = 106:16, Redfield et al., 1963). The calculation of $m_{P,I}$ is based on the

Table 1
Size-based parameter values

Parameter	Relationship
Plankton C content[1]	$m_{P,C}$, $m_{Z,C} = 1.32V^{0.758}$ mol C cell^{-1}
Plankton N content	$m_{P,N}$, $m_{Z,N} = 1.32V^{0.758}$ (16/106) mol N cell^{-1}
Plankton energy content	$m_{P,I} = 1.32V^{0.758}$ (1060/106) mol photon cell^{-1}
Maximum uptake rate of N	$k_N = \psi DN$ mol N cell^{-1} s^{-1}
Diffusion shape factor	$\psi = 4\pi r$ m cell^{-1}
Maximum uptake rate of I	$k_I = \overline{aA}I$ mol photon cell^{-1} s^{-1}
Chlorophyll concentration[2]	$C = 10^{(-1.678 - 0.310\log(V \times 10^{18}) + 9)}$ mg Chl a m^{-3}
Absorption cross section	$\overline{aA} = \pi r^2\left(1 - \frac{2(1-(1+2\gamma Cr)e^{-2\gamma Cr})}{(2\gamma Cr)^2}\right)$ m^2 cell^{-1}
Maximum growth rate of P[3]	$\mu_P^{max} = 8.06 \times 10^{-8} V_P^{-0.15}$ s^{-1}
Maximum growth rate of Z[4]	$\mu_Z^{max} = 2.40 \times 10^{-8} V_Z^{-0.21}$ s^{-1}
Encounter rate of P and Z	$\phi = \phi_{diff} + \phi_{vel} + \phi_{shear}$ m^3 s^{-1} cell^{-1}
ϕ due to diffusion	$\phi_{diff} = (2k_B T/3\eta)((1/r_P)+(1/r_Z))\times(r_P + r_Z)$ m^3 s^{-1} cell^{-1}
ϕ due to relative velocity	$\phi_{vel} = 0.5\pi r_P^2 U$ m^3 s^{-1} cell^{-1}
ϕ due to turbulent shear	$\phi_{shear} = 9.8(p^2/(1+2p)^2)(\epsilon/\nu)^{0.5}\times(r_P + r_Z)^3$ m^3 s^{-1} cell^{-1}
Sinking velocity of P[5]	$w_P = 2.48 \times 10^{-2}(100 r_P)^{1.17}$ m s^{-1}
Swimming velocity of Z[4]	$U_Z = 10^{-0.76 + 0.59\log r_Z}$ m s^{-1}
Sinking velocity of Z[5]	$w_Z = 2.48 \times 10^{-2}(100 r_Z)^{1.17}$ m s^{-1}

References: [1]Hofmann et al. (2000), [2]Finkel (2001), [3]Tang (1995), [4]Hansen et al. (1997), [5]Kiørboe (1993). r_P and V_P are the equivalent spherical radius and volume of the phytoplankton [m, m^3], $V = (4/3)\pi r^3$, r_Z and V_Z are the equivalent spherical radius and volume of the zooplankton [m, m^3], $\gamma = 0.04$ m^2 (mg Chl a)$^{-1}$ is the chlorophyll-specific absorption coefficient (Finkel and Irwin, 2000). D is the molecular diffusivity of nitrate [m^2 s^{-1}], ν is the kinematic viscosity [m^2 s^{-1}], η is the dynamic viscosity [kg s^{-1} m^{-1}], $k_B = 1.38 \times 10^{-23}$ J K^{-1} is the Boltzmann constant, U is the relative encounter velocity of cells based on Baird and Emsley (1999), Eqs. (40)–(42), $p = r_P/r_Z$, ϵ is the rate of dissipation of turbulent kinetic energy [m^2 s^{-3}], and I is the irradiance quantified as a photon flux [mol photon m^{-2} s^{-1}].

quantum yield of photosynthesis. The theoretical maximum is 0.125 mol C (mol photon)$^{-1}$. A more realistic value of 0.1 mol C (mol photon)$^{-1}$ has been used (Kirk, 1994).

The local time derivatives of the biological state variables are:

$$F_N = \underbrace{-k_N\left(\frac{R_N^{max} - R_N}{R_N^{max}}\right)\frac{P}{m_{P,N}}}_{\text{uptake by phytoplankton}} \underbrace{+\zeta_P P + \zeta_P R_N \frac{P}{m_{P,N}} + \zeta_Z Z}_{\text{regeneration}} \underbrace{+\gamma\min\left[\phi P/m_{P,N}, \frac{\mu_Z^{max}}{(1-\gamma)}\right]Z + \min\left[\phi P/m_{P,N}, \frac{\mu_Z^{max}}{(1-\gamma)}\right]Z\frac{R_N}{m_{P,N}}}_{\text{sloppy grazing}} \quad (3)$$

$$F_{R_N} = \underbrace{+k_N\left(\frac{R_N^{max} - R_N}{R_N^{max}}\right)}_{\text{DIN uptake}} \underbrace{-\mu_P^{max}(m_{P,N} + R_N)\frac{R_N}{R_N^{max}}\frac{R_I}{R_I^{max}}}_{\text{phytoplankton growth}} \quad (4)$$

$$F_{R_I} = \underbrace{+k_I\left(\frac{R_I^{max} - R_I}{R_I^{max}}\right)}_{\text{light capture}} \underbrace{-\mu_P^{max}(m_{P,I} + R_I)\frac{R_N}{R_N^{max}}\frac{R_I}{R_I^{max}}}_{\text{phytoplankton growth}} \quad (5)$$

$$F_P = \underbrace{+\mu_P^{max}\frac{R_N}{R_N^{max}}\frac{R_I}{R_I^{max}}P}_{\text{phytoplankton growth}} \underbrace{-\min\left[\phi P/m_{P,N}, \frac{\mu_Z^{max}}{(1-\gamma)}\right]Z}_{\text{grazing}} \underbrace{-\zeta_P P}_{\text{regeneration}} \quad (6)$$

$$F_Z = \underbrace{+\min\left[\phi P/m_{P,N}, \frac{\mu_Z^{max}}{(1-\gamma)}\right]Z - \gamma\min\left[\phi P/m_{P,N}, \frac{\mu_Z^{max}}{(1-\gamma)}\right]Z}_{\text{grazing}} \underbrace{-\zeta_Z Z}_{\text{regeneration}} \quad (7)$$

where k_N and k_I are the maximum rates of DIN and energy uptake of phytoplankton, respectively (and are a function of N and incident light, respectively), R_N^{max} and R_I^{max} are the maximum values of R_N and R_I, respectively, μ_P^{max} and μ_Z^{max} are the maximum growth rates of phytoplankton and zooplankton, respectively, ϕ is the encounter rate coefficient between phytoplankton and zooplankton, ζ_P and ζ_Z are the mortality rates of phytoplankton and zooplankton, respectively, and $(1-\gamma)$ is the assimilation efficiency of grazing. The local time derivatives of F_N, F_P and F_Z have units of mol N m^{-3} s^{-1}, while F_{R_N} has units of mol N cell^{-1} s^{-1}, and F_{R_I} has units of mol photon cell^{-1} s^{-1}. The term $P/m_{P,N}$ which appears in the DIN uptake and the phytoplankton grazing terms, is the number of phytoplankton cells.

Note that the total mass of nitrogen reserves in the model depends on both R_N and P. When phytoplankton grow (that is, nitrogen is exchanged between R_N and P), the loss from R_N in Eq. (4) is given by the growth rate, $\mu = \mu_P^{max}(R_N/R_N^{max})(R_I/R_I^{max})$, multiplied by $m_{P,N} + R_N$, while the gain in phytoplankton biomass in Eq. (6) is given by the growth rate multiplied by P. Note firstly that the loss

in R_N is multiplied by $m_{P,N}$ to convert the growth rate to a flux of N per cell, while the gain in phytoplankton biomass is multiplied by P to account for the change in the total phytoplankton biomass. Beyond this unit change, the greater loss in R_N than gain in P (the addition of R_N to $m_{P,N}$ in Eq. (4)) can be accounted for by the sharing of nitrogen reserves among the now greater number of phytoplankton cells. This effect is common to all cell quota models, and is referred to as "dissipation by cell multiplication" in Droop (1983).

In contrast to growth, mortality of phytoplankton (through regeneration or grazing) results in no change in the nitrogen reserves. In the model, it is assumed that the nitrogen reserves of the phytoplankton lost to grazing are released to DIN at the grazing rate, $\min[\phi P/m_{P,N},\ (\mu_Z^{max}/(1-\gamma))]Z$, multiplied by the reserves fraction ($R_N/m_{P,N}$). The sloppy grazing term in Eq. (3) becomes the loss due to inefficient assimilation of phytoplankton biomass by zooplankton grazing, $\gamma\min[\phi P/m_{P,N},\ (\mu_Z^{max}/(1-\gamma))]Z$, added to the release of nitrogen reserves. Similarly, the natural mortality (or regeneration) of phytoplankton, at a rate $\zeta_P P$ returns nitrogen to the dissolved inorganic pool at a rate of $\zeta_P(1+(R_N/m_{P,N}))P$ to account for the nitrogen reserves in the lost phytoplankton cells.

3.2. Conservation of mass

The total concentration of nitrogen in the biological state variables at a point in space is given by:

$$\text{mass} = N + P + \frac{R_N P}{m_{P,N}} + Z. \tag{8}$$

The third term on the right-hand side of Eq. (8), the reserves of one cell multiplied by the number of cells, accounts for the nitrogen stored in all phytoplankton cells as nitrogen reserves. The conservation of mass in biological model described by Eqs. (3)–(7) can be illustrated by taking the time derivatives of the terms in Eq. (8) when all spatial derivatives are set to zero:

$$\frac{\partial N}{\partial t} + \frac{\partial P}{\partial t} + \frac{\partial (R_N P/m_{P,N})}{\partial t} + \frac{\partial Z}{\partial t} = F_N + F_P + \left(\frac{F_P R_N}{m_{P,N}}\right) + \left(\frac{PF_{R_N}}{m_{P,N}}\right) + F_Z \tag{9}$$

using the product rule to differentiate the third term on the left-hand side. The third and fourth terms of the right hand of Eq. (9) can be calculated from Eqs. (4) and (6), respectively:

$$\frac{F_P R_N}{m_{P,N}} = +\mu_P^{max}\frac{R_N}{R_N^{max}}\frac{R_I}{R_I^{max}}\frac{PR_N}{m_{P,N}} - \min\left[\phi P/m_{P,N}, \frac{\mu_Z^{max}}{(1-\gamma)}\right]\frac{ZR_N}{m_{P,N}} - \zeta_P\frac{PR_N}{m_{P,N}} \tag{10}$$

$$\frac{PF_{R_N}}{m_{P,N}} = +k_N\left(\frac{R_N^{max}-R_N}{R_N^{max}}\right)\frac{P}{m_{P,N}} - \mu_P^{max} m_{P,N}\frac{R_N}{R_N^{max}}\frac{R_I}{R_I^{max}}\frac{P}{m_{P,N}} - \mu_P^{max} R_N\frac{R_N}{R_N^{max}}\frac{R_I}{R_I^{max}}\frac{P}{m_{P,N}} \tag{11}$$

The substitution of terms from Eqs. (3), (6), (7), (10) and (11) into Eq. (9) shows that all terms in Eq. (9) cancel, demonstrating conservation of mass.

The spatial derivatives of the biological state variables can now be introduced to form the full advection–diffusion-reaction equations:

$$\frac{\partial N}{\partial t} + \mathbf{v}\cdot\nabla N = \frac{\partial}{\partial x}\left(K_H\frac{\partial N}{\partial x}\right) + \frac{\partial}{\partial z}\left(K_V\frac{\partial N}{\partial z}\right) + F_N \tag{12}$$

$$\frac{\partial P}{\partial t} + \mathbf{v}\cdot\nabla P = \frac{\partial}{\partial x}\left(K_H\frac{\partial P}{\partial x}\right) + \frac{\partial}{\partial z}\left(K_V\frac{\partial P}{\partial z}\right) + F_P - w_P\frac{\partial P}{\partial z} \tag{13}$$

$$\frac{\partial Z}{\partial t} + \mathbf{v}\cdot\nabla Z = \frac{\partial}{\partial x}\left(K_H\frac{\partial Z}{\partial x}\right) + \frac{\partial}{\partial z}\left(K_V\frac{\partial Z}{\partial z}\right) + F_Z - w_Z\frac{\partial Z}{\partial z} \tag{14}$$

$$\frac{\partial (PR_N)}{\partial t} + \mathbf{v}\cdot\nabla (PR_N) = \frac{\partial}{\partial x}\left(K_H\frac{\partial (PR_N)}{\partial x}\right) + \frac{\partial}{\partial z}\left(K_V\frac{\partial (PR_N)}{\partial z}\right) + F_{R_N}P + F_P R_N - w_P\frac{\partial (PR_N)}{\partial z} \tag{15}$$

$$\frac{\partial(PR_I)}{\partial t} + \mathbf{v}\cdot\nabla(PR_I) = \frac{\partial}{\partial x}\left(K_H\frac{\partial(PR_I)}{\partial x}\right) + \frac{\partial}{\partial z}\left(K_V\frac{\partial(PR_I)}{\partial z}\right) + F_{R_I}P + F_P R_I - w_P\frac{\partial(PR_I)}{\partial z} \quad (16)$$

where F_N, F_{R_N}, F_{R_I}, F_P and F_Z are the local rates of change defined in Eqs. (3)–(7), the symbol $\nabla=((\partial/\partial x),(\partial/\partial z))$, $\mathbf{v}$ is the velocity field, K_H and K_V are the horizontal and vertical eddy diffusion coefficients, respectively, and w_P and w_Z are the sinking velocities of phytoplankton and zooplankton, respectively. Note that the equations for R_N and R_I consider the total nitrogen and energy held as reserves, (PR_N) and (PR_I), respectively, as it is the total nitrogen and energy that must be conserved. After the above equations have been solved, the values for R_N and R_I can be calculated from $R_N=(PR_N)/P$ and $R_I=(PR_I)/P$.

3.3. Light attenuation

The light attenuation coefficient through a layer of water is given by:

$$K_d = k_w + n_P\overline{aA} \quad (17)$$

where k_w is the attenuation coefficient of water (Table 2), n_P is the number of phytoplankton cells, and is given by $n_P=P/m_{P,N}$, and $\overline{aA}$ is the absorption cross section of the phytoplankton cells (Table 1). The bar above aA signifies that the parameter represents the mean absorption cross section of a phytoplankton cell over a random orientation (Baird, 2003). The light at the bottom of a layer dz thick is given by:

$$I_{bot} = I_{top}e^{-K_d dz} \quad (18)$$

and the average light within the layer is given by:

$$I = \frac{I_{top} - I_{bot}}{K_d dz}. \quad (19)$$

Table 2
Model constants

Parameter	Symbol	Value	Units
Molecular diffusivity of N	D	19×10^{-10}	$m^2\ s^{-1}$
Attenuation coefficient of water	k_w	0.04	m^{-1}
Reference temperature	T_{ref}	20	°C
Temperature coefficient	Q10	2.0	–

The value for D is at $T=25$ °C, $S=35$ ppt. In the simulations, D varies with temperature and salinity.

3.4. Temperature dependence

The molecular diffusivity of nitrate, D, and the kinematic viscosity, v, have a temperature dependence given in Li and Gregory (1974) and Wolf-Gladrow and Riebesell (1997). Maximum growth rate parameters, μ_P and μ_Z, have an exponential temperature dependence given by:

$$\mu = \mu_{T_{ref}}Q10^{(T-T_{ref})/10} \quad (20)$$

where T_{ref} is the reference temperature and Q10 is the temperature coefficient.

3.5. Size-based determination of biological parameter values

Most of the parameters in the biomechanical descriptions of biological processes are dependent on the size of planktonic cells (Table 1). Only a few are not size-dependent, and can generally be considered as constants (Table 2). As a result, the model simulations are specified primarily by the radius of the plankton species. It should be noted that the allometric relationships which define the amount of chlorophyll per cell, C, the plankton C content, m_C, and the maximum growth rate of phytoplankton, μ_P^{max}, and zooplankton, μ_Z^{max}, do contain empirical coefficients (Table 1). Allometric studies are highly valued in the biological literature. Typically scientists dedicate much effort to these studies, and publish relationships based on large sample sizes. For example, the allometric relationship for phytoplankton growth rate, μ_P^{max}, is based on 127 measurements from 69 different species (Tang, 1995). While such relationships contain inherit biological variability, large sample sizes ensure a meaningful relationship (in the case of μ_P^{max}, $r^2=0.34$, $p<0.0001$). Furthermore, since the allometric relationships are independent of the modelling

study, there can be no direct bias in the parameter determination, except in the choice of plankton radii.

3.6. Biological parameter values in the simulations

In order to facilitate comparisons between the Franks and biomechanical models, planktonic sizes have been calculated so that the magnitude and derivative of the biomechanical descriptions of DIN uptake and predator–prey encounter rates at zero and infinite DIN and phytoplankton concentration, respectively, are equal to those of the empirical descriptions in the Franks model. These calculations are detailed in Appendix C. For example, the radius of a phytoplankton cell has been calculated in order that the slope of DIN uptake rate against DIN concentration at zero DIN concentration in the biomechanical description is the same as that of the Franks model. Using the Edwards et al. (2000a) microzooplankton parameter set, these calculations produce a phytoplankton radius, r_P, of 5 μm and a relative encounter velocity between predators and prey, U, of 180 μm s^{-1} (Appendix C). A commonly observed phytoplankton species present in the East Australian Current is *Thalassiosira partheneia* (Dela-Cruz et al., 2002, 2003), a small centric diatom of 8–13 μm diameter (Bax et al., 2001). The predator species is assumed to have a radius, r_Z, 10 times the radius of the prey species, which lies between that found for ciliates (8 ×) and copepods and rotifers (18 ×) (Hansen et al., 1994). The zooplankton radius, r_Z, is therefore 50 μm. The calculated relative encounter velocity of 180 μm s^{-1} is within the range of 100–1000 μm s^{-1} range found for zooplankton species with a radius of 50 μm (Hansen et al., 1997). As zooplankton swimming velocities are likely to be much greater than phytoplankton swimming velocities, the relative encounter velocity due to swimming can be assumed to be equal to the zooplankton swimming speed. Fitting the Hansen et al. (1997) data to a power law would predict a swimming velocity of a 50 μm radius zooplankton cell of 560 μm s^{-1}.

For parameters which appear in both the biomechanical and Franks models, such as the maximum growth rate of phytoplankton, the values of the Edwards et al. (2000a) microzooplankton parameter set have been used in simulations of both the biomechanical and Franks models (Table 3). Where a size-based relationship is available, the value given by the

Table 3
Parameter values used in the simulations

Parameter	Symbol	Value	Units
Biomechanical parameters calculated using mathematical similarities with the Franks model and using the Edwards et al. (2000a) microzooplankton parameter set			
Phytoplankton radius	r_P	5	μm
Zooplankton radius	r_Z	50	μm
Maximum relative encounter velocity	U	180 (560)	μm s^{-1}
Parameters obtained directly from the Edwards et al. (2000a) microzooplankton parameter set			
Assimilation coefficient	γ	0.3	–
Phytoplankton mortality	ζ_P	0.1	day^{-1}
Zooplankton mortality	ζ_Z	0.2	day^{-1}
Maximum growth rate of P	μ_P^{max}	2.0 (1.36)	day^{-1}
Maximum growth rate of Z	μ_Z^{max}	4.0 (0.78)	day^{-1}
Sinking rate of P	w_P	0.0 (0.29)	m day^{-1}
Sinking rate of Z	w_Z	0.0 (4.35)	m day^{-1}
Parameters unique to the biomechanical model and based on r_P and r_Z			
Phytoplankton N content	$m_{P,N}$	5.21×10^{-13}	mol N $cell^{-1}$
Phytoplankton energy content	$m_{P,I}$	3.45×10^{-11}	mol I $cell^{-1}$
Maximum phytoplankton N reserves	R_N^{max}	5.21×10^{-13}	mol N $cell^{-1}$
Maximum phytoplankton energy reserves	R_I^{max}	3.45×10^{-11}	mol I $cell^{-1}$
Zooplankton N content	$m_{Z,N}$	9.78×10^{-11}	mol N $cell^{-1}$
Diffusion shape factor	ψ	6.28×10^{-5}	m $cell^{-1}$
Phytoplankton Chl concentration	C	3.01×10^{6}	mg Chl m^{-3}
Absorption cross section	$\overline{aA}$	7.85×10^{-11}	m^2 $cell^{-1}$
Phytoplankton Chl/ N ratio	CV/m_N	3.03	(mg Chl *a*/ (mmol N))$^{-1}$

The first three parameters are calculated in Appendix C from a comparison of the biomechanical and Franks model descriptions. The next seven parameters have identical definitions in the biomechanical and Franks models, and are based on the Edwards et al. (2000a) study microzooplankton parameter set. Bracketed values represent the values these parameters would take using the size-based relationships in Table 1, and are used in the supplementary simulations. The final nine parameters are unique to the biomechanical model and are obtained from the size-based relationships (Table 1) using $r_P = 5$ μm and $r_Z = 50$ μm.

size-based relationship is bracketed in Table 3, and only used in the supplementary simulations.

Table 3 also lists the values of those parameters which are both unique to the biomechanical model and are determined from size-based relationships. These parameters include the stoichiometry coefficients of plankton cells m, the diffusion shape factor $\underline{\psi}$, the absorption cross section of phytoplankton cells $\overline{aA}$, and the maximum phytoplankton reserves of N, R_N^{max} and of energy, R_I^{max}. The parameters R_N^{max} and R_I^{max} are assumed to be equal to m_N and m_I, respectively. Under such an assumption, phytoplankton cells are capable of storing as much nitrogen and energy as is required in order to complete a cell division. Alternatively, this could be viewed as cells being able to vary their C/N ratio from half to twice that of the Redfield ratio.

3.7. Biological forcing and boundary conditions

The biology is forced with cloudless PAR irradiance calculated at every physical time step based on astronomical cycles for 31°S (Brock, 1981). Otherwise there is no external forcing of the biology except through the physical properties of T, S and the TKE dissipation rate, ϵ. The boundary conditions at the surface, bottom and coast are zero flux boundary conditions. The alongshore boundary conditions are periodic for all variables to ensure uniformity in the alongshore direction. As a result, the mass of nitrogen in the model domain remains constant throughout the simulations.

3.8. Biological initial conditions

The initial (for Day-375) DIN field is interpolated from the annual averages of the CSIRO Atlas of Regional Seas (Ridgway et al., 2002) at 30°S 153.5°E. At 50 m depth, the annual average DIN concentration is 1.7×10^{-3} mol N m^{-3}. There is little data to use for the initialisation of phytoplankton and zooplankton concentrations. For the purposes of this study, total nitrogen is assumed to be constant above 50 m. The initial phytoplankton and zooplankton concentrations are then both set to half of the difference between the annual DIN of that depth and 1.7×10^{-3} mol N m^{-3}. Below 50 m, initial phytoplankton and zooplankton concentrations are both set to 0.

See Appendix B for details of the numerical methods.

4. Results

The model results are given by the value of the state variables and the rate of processes (or equation terms) averaged over an inertial period ($=|2\pi/f|=1.028$ day, where $f=-7.07\times10^{-5}$ s^{-1} is the Coriolis parameter) to highlight the development of subinertial phenomena. The model results on Day 0 show the value of the state variables after 375 days with a stable surface mixed layer. The results from Day 0 to Day 20 show the effect over time of upwelling favourable winds (after 375 days of oscillating winds) on the upwelling coast, a small portion of the whole model domain.

4.1. Physical response

Snapshots of the response of temperature, alongshore velocity, cross-shelf streamfunction, mean dissipation rate of TKE and the light field (as affected by the spatially distributed phytoplankton concentration) adjacent to the upwelling coast are given in Fig. 2 for Days 0, 5, 10, 15 and 20. Over the 375-day spin-up period of sinusoidally oscillating winds a surface mixed layer with a depth of approximately 20 m forms with no net horizontal transport of water. The temperature and salinity profiles remain approximately constant over the spin-up period (due to nudging to initial conditions) except in the surface mixed layer, which becomes vertically well mixed.

After 375 days of the varying winds, a constant northerly wind stress of 0.05 N m^{-2} is applied. In the Southern Hemisphere, this wind is upwelling favourable on the western edge of the ocean basin. The response is similar to that of the Edwards et al. (2000a) study. On the western side of the ocean basin, an offshore Ekman transport quickly develops in the surface mixed layer of the water column, as shown by the eastward advection of warm surface water and the negative cross-shelf streamfunction. Initially the return flow occurs throughout the water column below the surface mixed layer (not shown), but within 3–4 days the flow becomes concentrated within a 5-m-thick bottom boundary layer (see the cross-shelf

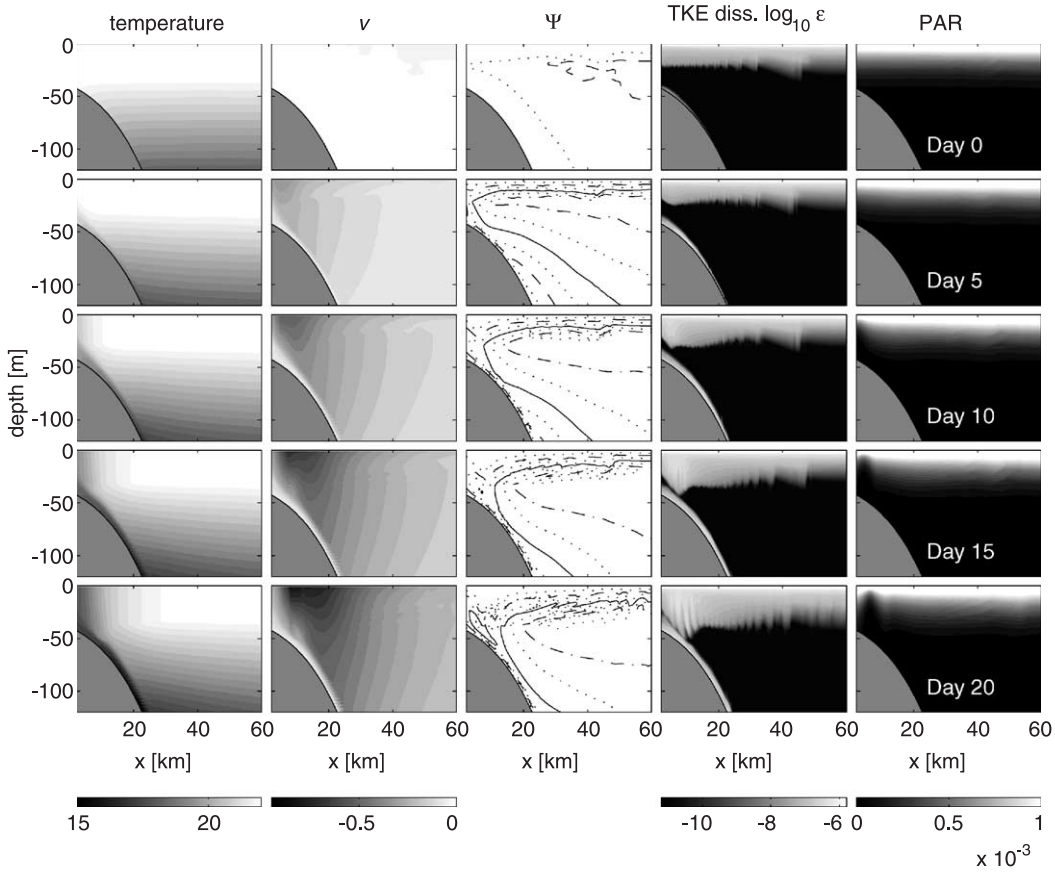

Fig. 2. The physical state variables: temperature [°C], alongshore velocity, v [m s^{-1}], cross-shelf streamfunction, ψ [m^2 s^{-1}], TKE dissipation rate, ϵ [m^2 s^{-3}] and photosynthetically available radiation, PAR, [mol photon m^{-2} s^{-1}]. The cross-shelf streamfunction field has been interpolated from a sigma to a Cartesian coordinate system for plotting. The lines on the cross-shelf streamfunction represent -0.1 (· · ·), -0.2 (- -), -0.3 (· · ·), -0.4 (-), -0.5 (· · ·), -0.6 (·-), -0.7 (· · ·) m^2 s^{-1}, where negative represent velocities in a clockwise sense. PAR is a function of the spatial distribution of phytoplankton cells, and is from the simulation in Fig. 3.

streamfunction on Day 5 in Fig. 2). A corresponding increase in TKE dissipation rate in the surface mixed layer and bottom boundary layer can be seen. The maximum inertially averaged TKE dissipation rates during the upwelling event in the surface mixed layer and bottom boundary layer are 2.0×10^{-5} and 7.3×10^{-5} m^2 s^{-3}, respectively, and are of the same order as observed values (Craig and Banner, 1994). Over the course of the upwelling period, isotherms become uplifted over the shelf, and a strong baroclinic coastal jet develops. The spatial distribution and magnitude of the alongshore current is very similar to that found in Allen et al. (1995). For a more thorough description of coastal upwelling in a 2D model using the Princeton Ocean Model, see Allen et al. (1995). Two-dimensional simulations typical of Australia's east coast have also been undertaken (Marchesiello et al., 2000).

4.2. Biological response of the biomechanical model

4.2.1. Response to a stable surface mixed layer

Snapshots of the biological state variables on Day 0 after 375 days of oscillating winds can be seen in the top row of Fig. 3. The biological state variables at Day 0 are relatively uniform in the cross-shelf direction. A broad deep chlorophyll maximum (DCM) develops between depths of 20 and 70 m. The maximum of

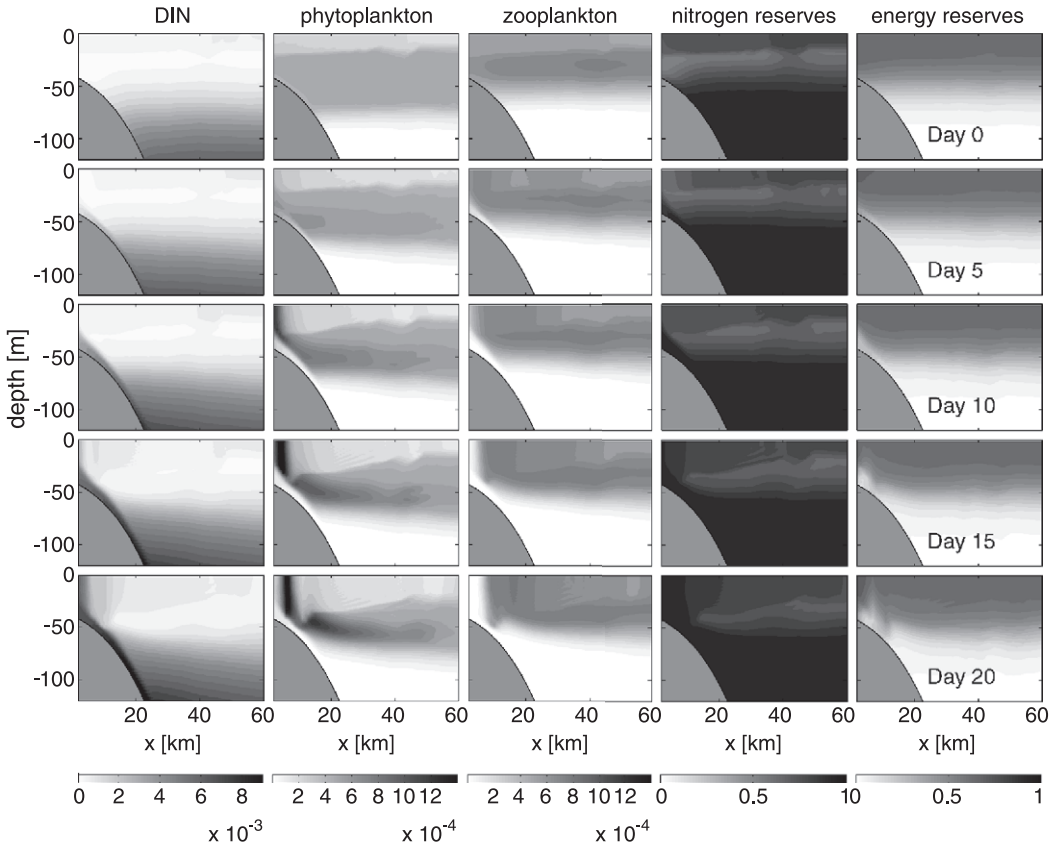

Fig. 3. The biological state variables: dissolved inorganic nitrogen (DIN), phytoplankton, and zooplankton concentrations [mol N m^{-3}]. The nitrogen and energy reserves are normalised to their maximum values, to give a value between 0 and 1.

10^{-3} mol N m^{-3} corresponds to a chlorophyll concentration of ≈ 3 mg Chl m^{-3} (Table 3). The zooplankton concentration is relatively constant between the surface and a depth of 50 m, and drops off quickly with depth below 50 m. There is a hint of a maximum for zooplankton at a depth of 40 m.

The DCM develops as a result of the presence of a surface mixed layer, and the effect this has on phytoplankton processes. The DCM formation can be understood by examining the evolution over time of the vertical profiles of the rates of phytoplankton processes. The local rate of change in a state variable with time ($\partial N/\partial t$, $\partial P/\partial t$,... etc.) is called the tendency term, and represents the sum of the physical and biological processes, both positive and negative, affecting the state variable. Positive and negative tendencies correspond to increases and decreases, respectively, in the value of the state variable at a fixed point.

Fig. 4 graphs for Days −375, −370, −365, −360 and −305 the vertical profile of the phytoplankton terms and biomass at the centre of the model domain (75 km from both coasts in 400 m of water) for the simulation in Fig. 3. The initial profile shows no DCM. On Day −370, the phytoplankton tendency is negative in the top 20 m, becoming strongly positive at approximately 40 m, and reducing to zero at 60 m. In the top 20 m, grazing losses increase dramatically close to the surface, where encounter rates are enhanced by high rates of dissipation of TKE. This increase is partially balanced by vertical diffusion, resulting at Day −370 in a small negative tendency in the top 20 m. The strong positive tendency at 40 m results from strong phytoplankton growth and only weak grazing pressure, as encounters due to turbulent shear are reduced at depth. By Day −365, the phytoplankton biomass is now reduced in the top 20

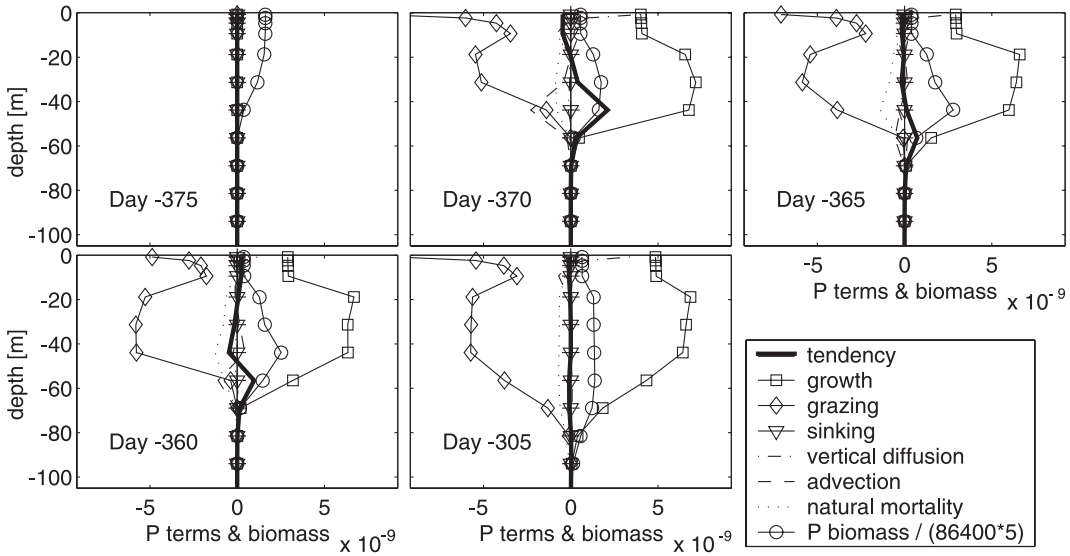

Fig. 4. The phytoplankton terms [mol N m^{-3} s^{-1}] and biomass [mol N m^{-3}] (divided by (86,400 × 5) s day^{-1}) at the centre of the domain for the main simulation shown in Fig. 3. The solid bold line is the phytoplankton tendency. By scaling biomass by 1/(86,400 × 5) day s^{-1}, the terms, if applied over a 5-day period, would result in a change in the scaled biomass equal to the magnitude of the terms themselves.

m due to the negative tendency over the previous 10 days, and increased at 40 m due to the positive tendency. This positive tendency persists at depth, its centre slowing migrating down the water column to 60 m at Day −360. As a result, a DCM forms from approximately 20 to 60 m. By Day −305, the phytoplankton tendency goes to zero as a balance between grazing and growth terms at each depth in the water column is established. Explicitly, the DCM forms because (1) under a uniform depth profile for phytoplankton biomass there is a positive tendency for phytoplankton biomass at depth relative to the surface, and (2) once the DCM has formed, there is no tendency for it to dissipate. The relative positive tendency at depth for a uniform depth profile arises due to phytoplankton growth being distributed deeper in the water column than zooplankton grazing loss.

At Day 0 in the surface mixed layer, phytoplankton growth is limited by both DIN uptake and light capture (as shown by both energy and nitrogen reserves being less than one). Interestingly, while energy reserves decrease with depth, nitrogen reserves have a minimum at ≈ 30 m, corresponding to the region of greatest primary productivity. Below the surface mixed layer, phytoplankton growth is strongly light limited.

4.2.2. Response to an upwelling favourable wind

The response to an upwelling favourable wind can be seen in the snapshots of the biological state variables from Days 5, 10, 15 and 20 (Fig. 3). Within 5–10 days, a phytoplankton bloom is evident in the surface mixed layer within a few kilometers of the coast. Over the next 15 days, the bloom develops as it is advected eastward by the offshore Ekman transport. The bloom develops throughout the surface mixed layer, and extends to the top of the developing bottom boundary layer. The offshore Ekman transport at Day 10 in the surface mixed layer is approximately 2 km day^{-1}, while the phytoplankton bloom is moving at ≈ 0.7 km day^{-1}, reaching a maximum of 1.9×10^{-3} mol N m^{-3} at a distance offshore of 7 km by Day 30 (not shown). The slower movement of the phytoplankton maximum is due to growth at the coastal edge and zooplankton grazing at its offshore edge. The zooplankton population is also advected offshore. From Days 10–20, the zooplankton maximum moves at about 1 km day^{-1}. For zooplankton, the slower movement is associated with growth at the coastal edge and mortality at the offshore edge. Zooplankton reaches a maximum concentration at an offshore distance of 10 km at Day 35 (not shown).

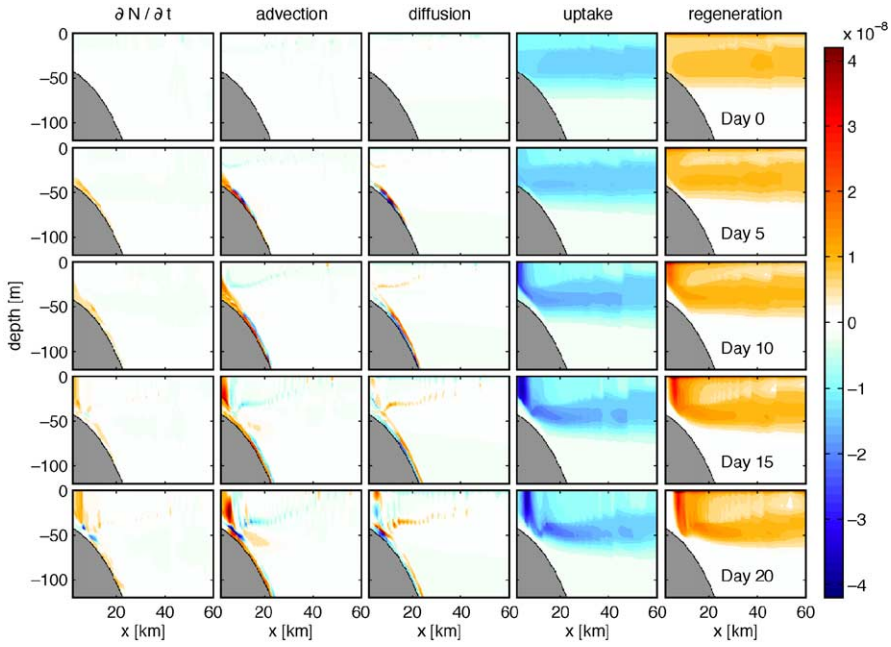

Fig. 5. The DIN terms: tendency, advection, vertical diffusion, uptake by phytoplankton and regeneration (including sloppy grazing) [mol N m^{-3} s^{-1}].

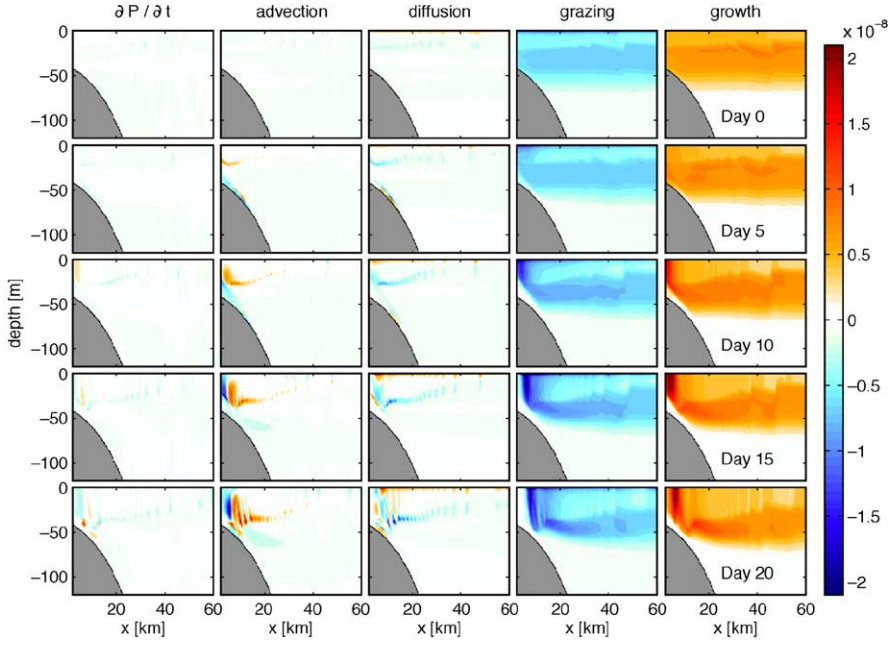

Fig. 6. The phytoplankton terms: tendency, advection, vertical diffusion, grazing by zooplankton and growth [mol N m^{-3} s^{-1}]. Natural mortality (not shown) is small relative to the other terms.

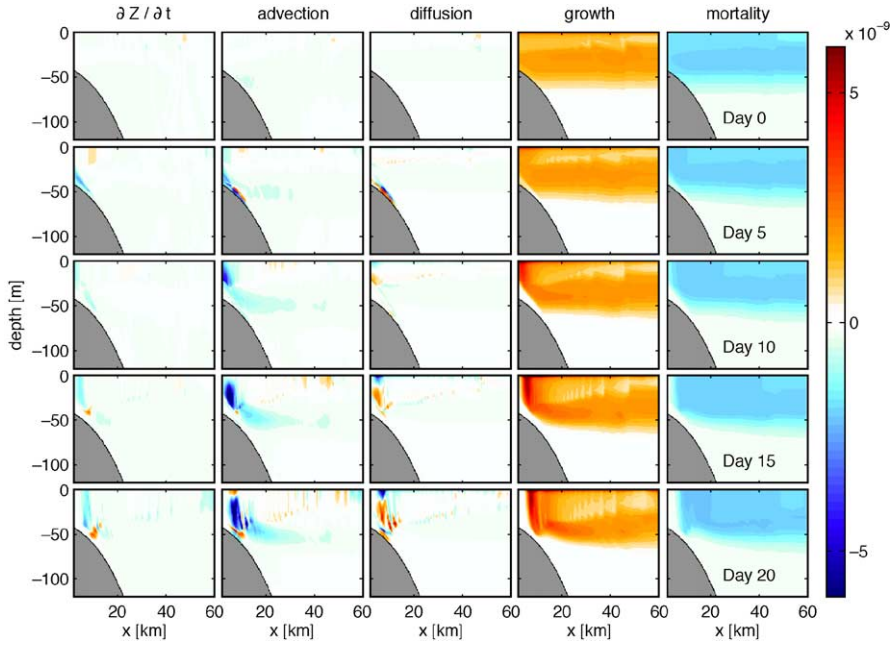

Fig. 7. The zooplankton terms: tendency, advection, vertical diffusion, growth and natural mortality [mol N m^{-3} s^{-1}].

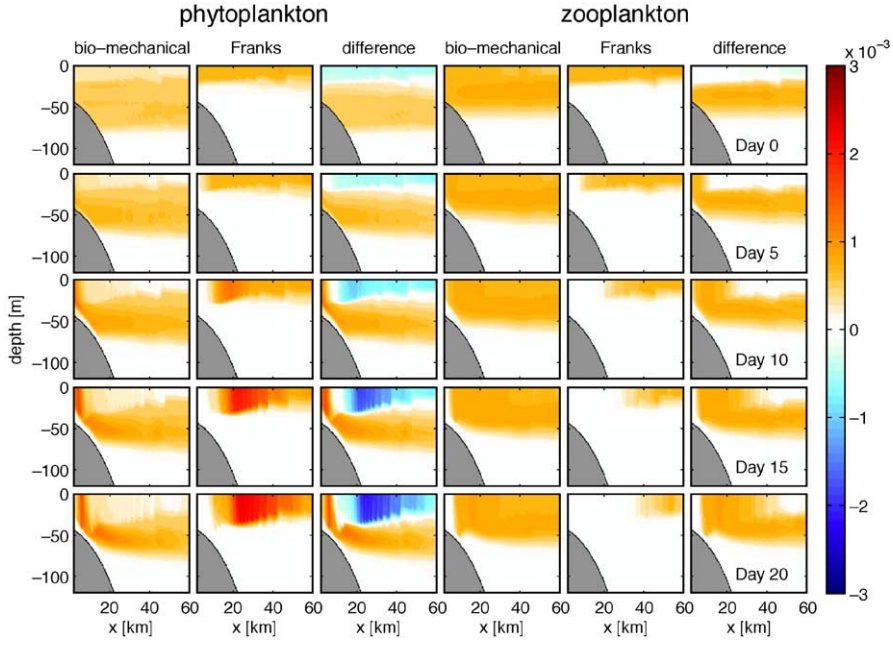

Fig. 8. The phytoplankton (left three columns) and zooplankton (right three columns) biomass for the biomechanical model, the Franks model with the Edwards study microzooplankton parameter set, and the difference [mol N m^{-3}].

A consideration of the internal reserves of energy and nitrogen gives an indication of changing limitations on primary productivity during upwelling. On Days 10–20, nitrogen reserves increase near the coast due to the upwelling of nutrient-rich water which is taken up by the phytoplankton. The increase in nitrogen reserves allows faster phytoplankton growth, although the faster growth, combined with reduced light due to self-shading, acts to reduce the energy reserves.

4.2.3. Analysis of the terms

Analysis of each of the terms in the biological equations (Eqs. (3)–(7)), as well as the advective and diffusive terms of each of the biological state variables can be used to further investigate the biological response (Figs. 5–7). Note that positive values are red, negative values are blue, and zero values white.

The tendency terms are generally smaller than the most significant physical or biological process, illustrating that processes often counteract each other. For example, diffusion tends to dilute hotspots of biological activity, while advection tends to shift the biological system away from a steady state, only for biological processes to resist such a change. As a further generalisation, the change in biological state variables is initially dominated by biological processes before the upwelling favourable winds are applied. Once the upwelling winds are applied, advection and diffusion become important in locations where strong spatial gradients in biological entities exist.

The DIN terms (Fig. 5) show that on Day 5 advection has become an important source of DIN within the bottom boundary layer. Vertical diffusion acts to dilute this supply of DIN. By Day 10, advection is an important source of DIN up to a depth of 25 m. The excess DIN is quickly taken up by the phytoplankton, resulting in only a small positive tendency in DIN concentration. By Day 15, advection and vertical diffusion are important around the coastal and bottom edges of the bloom. The largest tendency in DIN concentration occurs after Day 20 inshore of

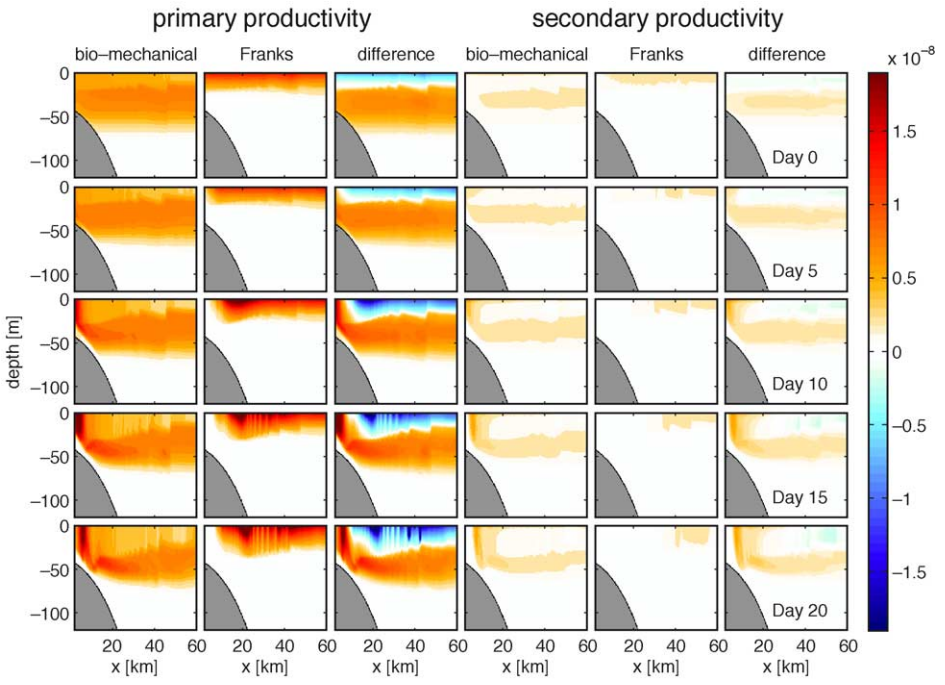

Fig. 9. The primary (left three columns) and secondary (right three columns) production for the biomechanical model, the Franks model with the Edwards study microzooplankton parameter set, and the difference [mol N m^{-3} s^{-1}].

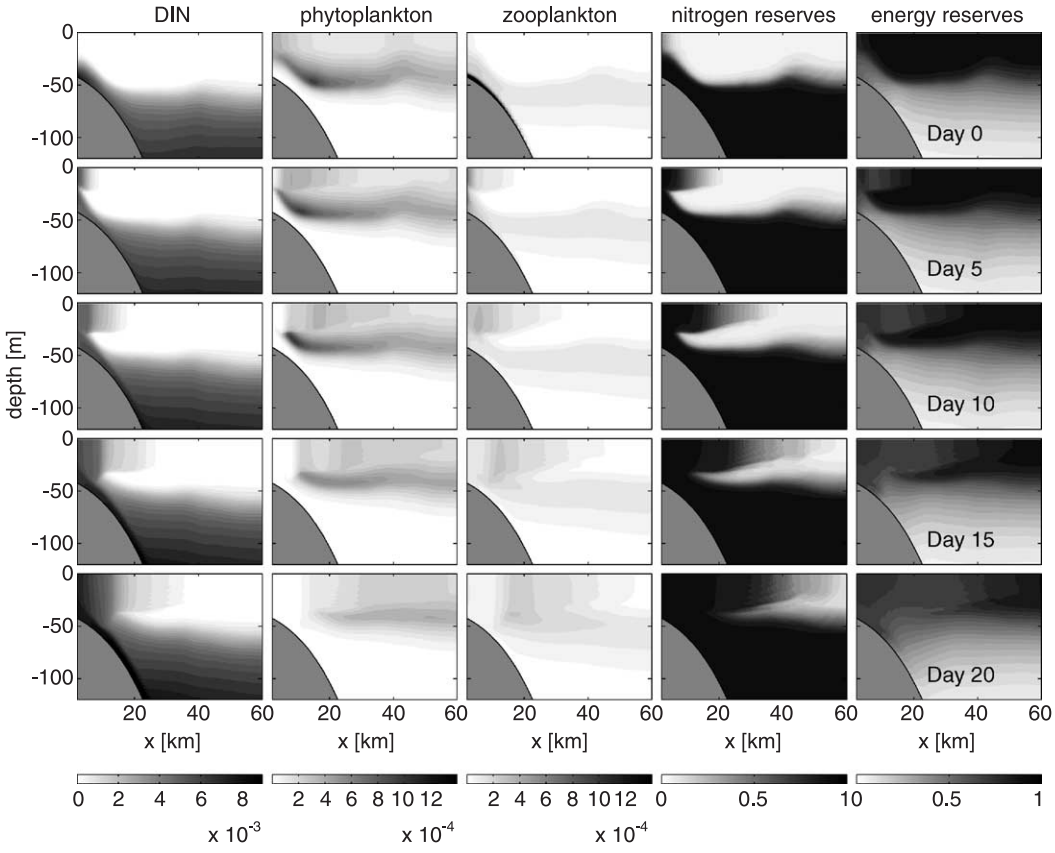

Fig. 10. The biological state variables for a simulation using allometric relationships only. For details, see Fig. 3.

the surface phytoplankton bloom. At this time, advection brings high DIN water to the surface, replacing the surface waters which were depleted of DIN. The local phytoplankton biomass is low, however, because the surface waters are being replaced by low phytoplankton concentration bottom waters, so uptake cannot balance advection, and hence the strong positive tendency.

The phytoplankton terms (Fig. 6) illustrate an increase in growth (of the whole population) by Day 5, becoming larger in magnitude and propagating offshore with time. Advection and vertical diffusion are important at the edge of the bloom, again tending to balance. The grazing term reaches a maximum at the offshore edge of the bloom, and accounts for the slower movement of the phytoplankton maximum than the velocity of the offshore Ekman current. As noted in the description of DCM formation, vertical diffusion is strongly positive in the top few meters, balancing the strong grazing loss due to high encounter rates of predators and prey in the turbulent surface waters. This effect becomes more pronounced as TKE dissipation rates increase under a constant wind stress and the higher velocity shears in the offshore Ekman current.

The zooplankton tendency (Fig. 7) is rarely positive, due primarily to large mortality losses and the advection of zooplankton in the offshore Ekman transport. Throughout the simulation, growth and mortality terms have similar spatial distributions, and so the zooplankton biomass does not vary spatially as much as the phytoplankton biomass. The strong grazing loss of phytoplankton in the surface waters corresponds to a large growth of zooplankton population. However, this gain is balanced by vertical diffusion losses in the top few meters.

4.3. Comparison of the biomechanical and Franks biological models

The simulations of the Franks model given in this paper use the microzooplankton parameter set of the Edwards et al. (2000a) study. For ease of comparison, the Franks model is coupled to the same physical model configuration as that to which the biomechanical model is coupled. In the Edwards et al. (2000a) study, the authors determine biological initial conditions by taking advantage of the analytical solution of the Franks model when light-limitation, advection, diffusion and sinking are not considered. In this study, the Franks model undergoes the same 'spin-up' as the biomechanical model and justification of this approach is made in the Discussion.

The concentrations of phytoplankton and zooplankton for the biomechanical model, the Franks model and the difference are given in Fig. 8. Under a stable surface mixed layer, the biomechanical model developed a DCM while the Franks model does not. When the upwelling begins, both models produce a surface bloom on the upwelling coast. The biomechanical model produces a phytoplankton bloom more quickly, and closer to the coast. By Day 20, the Franks model produces a larger bloom. The zooplankton response for the biomechanical model is larger, and is evident closer to the coast than the Franks model.

The rates of primary and secondary production in the biomechanical and Franks model are compared in Fig. 9. The differences in both primary and secondary production are mainly due to the different spatial

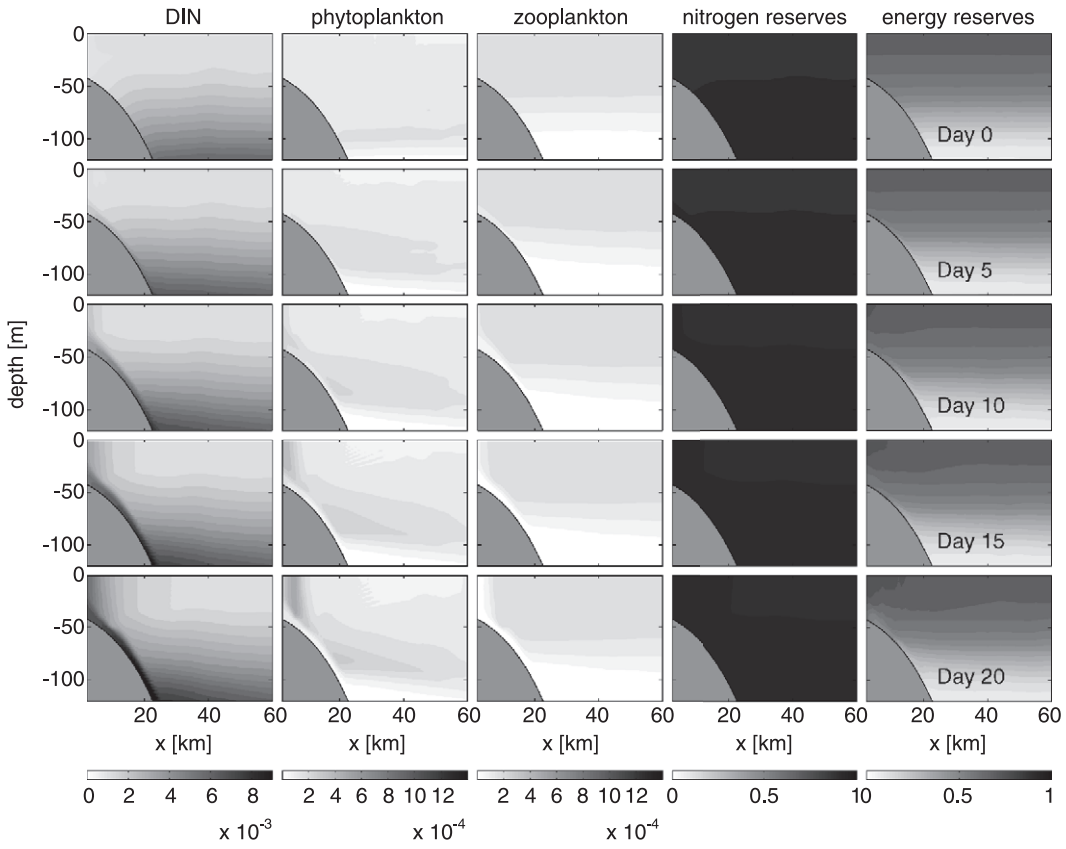

Fig. 11. The biological state variables for a simulation using allometric relationships only and no phytoplankton and zooplankton sinking. For details, see Fig. 3.

distributions of phytoplankton and zooplankton biomass. Most significantly, the Franks model shows little secondary productivity in the surface waters within 35 km of the coast, while the biomechanical model has its maximum at 7 km offshore.

4.4. Supplementary simulations with alternate parameter sets

The behaviour of the biomechanical model is further investigated by selecting different biological parameter values. The first supplementary simulation involves using the allometric relationships only to determine the parameter values. Retaining the phytoplankton and zooplankton radii from the earlier simulation, the maximum growth rates, sinking rates and relative encounter velocity are given by the bracketed values in Table 3. Fig. 10 displays snapshots of the biological variables on Days 0, 5, 10, 15 and 20 in the coastal upwelling region. With significant sinking velocities, the surface waters are more depleted of DIN. At Day 0, a stronger DCM can be seen than in the main simulation, and zooplankton concentration is lower, and located just below the DCM. When upwelling favourable winds are applied, a small response is seen in the surface phytoplankton as it is advected offshore. Notably a surface zooplankton maximum occurs around 20 km offshore.

A second supplementary simulation involves using allometric relationships only, but setting sinking rates of phytoplankton and zooplankton to zero (Fig. 11). Surface DIN values are now much higher, as well as the zooplankton biomass. In contrast the DCM is

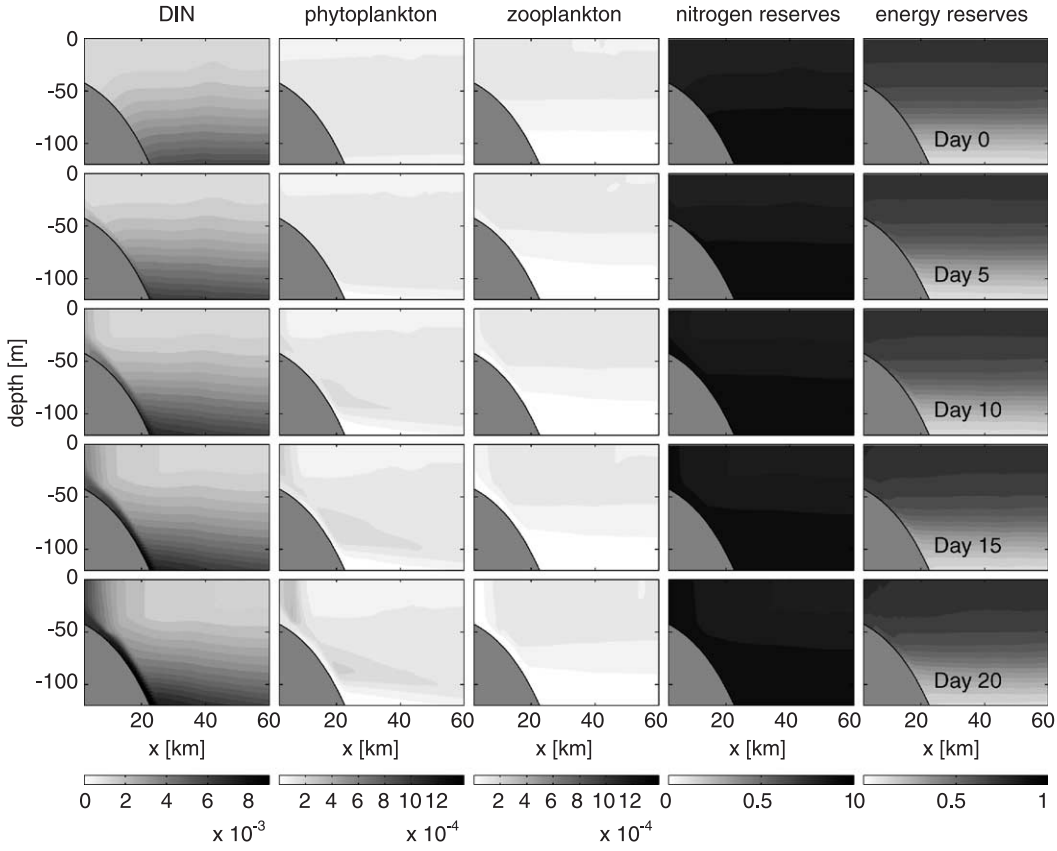

Fig. 12. The biological state variables for simulation using allometric relationships only and no phytoplankton and zooplankton sinking, and phytoplankton and zooplankton radii doubled ($r_P = 10$ μm and $r_Z = 100$ μm). For details, see Fig. 3.

weak, and phytoplankton biomass is less than in the two previous cases.

A third supplementary simulation involves using the allometric relationships with no sinking, but doubling the radius of the phytoplankton and zooplankton (Fig. 12). By doubling the cell radius, most of the derived parameters are changed. The most notable change in model output is the simulated phytoplankton and zooplankton biomasses are less. With a smaller phytoplankton surface area to volume ratio, DIN uptake rates are reduced, and phytoplankton have a slower maximum growth rate. The result is phytoplankton biomass reduced from all above cases. Zooplankton in turn has a lower biomass.

5. Discussion

This aim of this study is to model plankton populations using biomechanical descriptions of biological processes. This biomechanical model with radial dependencies of biological processes has the potential to link well with the many size-based studies of planktonic processes and size-based measurement techniques (optical plankton counters, image analysis of plankton collections and biomass size spectra analysis). The calculations described in Appendix C illustrate that the biomechanical model and the Franks model have mathematical similarities, despite the different approaches to their formulation. In particular, the calculation of realistic plankton radii in Appendix C suggests that the biomechanical descriptions used in the biomechanical model represent important limitations in pelagic ecosystems (Baird et al., 2003). Despite the similar physical model, and an attempt to choose plankton radii with rates of interaction that correspond to values in the Franks model, the Franks and biomechanical models behaviour is significantly different. This illustrates the importance of model formulation, in addition to parameter estimation, in determining model results.

The most significant advantage that the biomechanical model has over NPZ models with empirical descriptions, such as the Franks model, is in the ease of parameter estimation. Parameters used in empirical descriptions such as half-saturation constants take a wide range of values in different NPZ models. Often, realistic values are difficult to distinguish from unrealistic ones. The biomechanical model, in contrast, is based on cell radius, a physically meaningful parameter. The biomechanical model has the disadvantage (or is it an advantage?) that the calibration of biological processes to a particular environment is difficult because the primary tuneable parameters are the cell radii, which have only a relatively small range that would be considered reasonable. The biomechanical descriptions are also algebraically more complicated than empirical descriptions, and are based on the assumption that plankton processes proceed at a physical limit, which may not always be the case for natural systems. Physical limits are more likely to be important in nutrient or light impoverished environments (Baird et al., 2003), so their use in pelagic ecosystems such as the East Australian Current is justified.

Broadly speaking, the biomechanical model reproduced a number of the salient aspects of a coastal upwelling pelagic ecosystem. Under a stable surface mixed layer, a DCM of order 1.6 mg Chl m^{-3} formed, increasing to 6 mg Chl m^{-3} during upwelling events. DCMs are common in the East Australian Current and have similar magnitudes to the model (Roughan and Middleton, 2002). This demonstrates that the model is capturing the magnitude of the conversion of DIN to chlorophyll in the environmental conditions off the NSW coast.

5.1. Discussion of the DCM

The formation of a DCM due to elevated phytoplankton growth rates at depth, where both DIN and light are available in sufficient quantities, has been previously demonstrated in modelling studies (Sharples and Tett, 1994). The biomechanical model demonstrates an additional cause, a depth dependent decrease in predator–prey encounter rates due to decreased rates of TKE dissipation. This secondary cause may explain the presence of DCMs even when the limiting nutrient is supplied from the surface, such as observed during the Southern Ocean iron-release experiment (Boyd et al., 2000).

A DCM does not develop in the Franks model. The Franks model determines growth rate based on ambient light and DIN concentrations. As light decreases with depth through the water column, the maximum nutrient unlimited growth rate that phytoplankton can achieve decays with depth. In the Edwards et al.

(2000a) study, the actual phytoplankton growth rate always decreased with depth. In contrast, the biomechanical model incorporates light energy and nutrient into the cell. Growth rate is then determined by the balance of nutrient uptake, light capture and maximum growth rate. Under such as balance, given a depth dependent nutrient and light environment, the maximum growth rate and productivity can occur at depth.

5.2. Discussion of long duration model 'spin-up'

The decision to use a long duration 'spin-up' rather than an analytical solution for the initial state has proved valuable. When the Franks model with the Edwards et al. (2000a) microzooplankton parameter set is coupled to the physical configuration of this study with total nitrogen concentrations typical off Oregon (four times that of the east coast of Australia) it undergoes predator–prey oscillations. Edwards et al. (2000b) analysed the behaviour of the Franks model with realistic vertical diffusion (but no advection or sinking) and found similar limit cycle behaviour. Under such circumstances, it may be problematic to set initial conditions using a spin-up because the length of spin-up is critical in determining at what point in the limit cycle the simulation begins. The Edwards et al. (2000a) study took the most sensible alternative approach under these conditions of utilising analytical solutions for the biological model while recognising that physical processes are likely to alter this state as soon as the simulation begins.

Fortunately for this study, neither the Franks nor the biomechanical models undergo such oscillations in the nutrient-poor environmental conditions typical off the east coast of Australia. As a result, a long duration 'spin-up' becomes the most reasonable approach, as the biological variables can be said to have reached a quasi steady state that includes the effect of advection, diffusion and sinking. Interestingly, the biomechanical model does not undergo limit cycle behaviour at even five times the DIN concentrations observed off the east coast of Australia.

5.3. Discussion of supplementary simulations

The supplementary simulations using allometric relationships for maximum growth rates of phytoplankton and zooplankton, and for the encounter velocity, produced different results to the main simulation. The results appear reasonable, and may be preferred where data is available in order to assess results. In this paper, where a comparison with the Franks models provides the main method of model assessment, it is difficult to assess the relative performance using allometric relationships only. Nonetheless, the supplementary simulations show that (1) sinking is an important process which needs to be addressed further, especially with regard to the ability of zooplankton to maintain their position in the water column, and (2) that choice of cell radii does make a difference, but perhaps not as much as might have been expected. The simulations in Figs. 11 and 12 have cells with volumes a factor of 8 different, yet the results are not very different. This is due in part to the weak dependence of some biomechanical parameters on size. But it is also because the effect of radii on planktonic processes is mixed. For example, while increasing the cell radius increases a zooplankton cells encounter velocity for grazing, the cell's maximum growth rate decreases.

In conclusion, a simplification of the Baird and Emsley (1999) biomechanical model was coupled to a two-dimensional configuration of the Princeton Ocean Model. The results were comparable to, but different from, that of the commonly used Franks model. In particular, a DCM and a surface bloom within 10 km of the coast developed only in the biomechanical model. The ease of parameter estimation and the ability to capture DCMs make the biomechanical model well suited to studying pelagic ecosystems. This ability will be further explored by work in progress to couple the biomechanical model to a three-dimensional configuration of the Princeton Ocean Model for the NSW continental shelf (Oke and Middleton, 2001), and assess model performance against in situ and satellite measurements during the 1998–1999 austral summer (Roughan and Middleton, 2002).

Acknowledgements

This research was funded by an Australian Research Council (ARC) Discovery Project (DP0209193) held by I.M. Suthers and M.E. Baird. P.R. Oke was funded through an ARC grant to M.H. England. The use of the

Australian Partnership for Advanced Computing (APAC) supercomputer, scientific programming support of Clinton Chee (High Performance Computing Unit, UNSW), and insightful comments on a draft by B. B. Wallace are gratefully acknowledged. The helpful comments of two anonymous reviewers and C.V.W. Lewis have significantly improved the manuscript.

Appendix A. Idealised bathymetry

The idealised bathymetry is created using a hyperbolic tangent function:

$$h(x) = B + (A - B)\tanh\left(\left(\frac{x - C/2}{D}\right)^{E}\right) \qquad (21)$$

where $h(x)$ is the depth in meters at x km from the east coast in the x-direction. Eq. (21) describes an ocean basin with a minimum depth at the coast approaching A m as $|x - C/2| \gg D$, a maximum depth in the centre of the domain of B m, and a total width of C km. The fraction of the basin which is composed of the continental slope (as opposed to deep ocean or continental shelf) increases as the power E is increased, where E is an even positive integer. The approximate length of the deep ocean compared to the shallow continental shelf is determined by D. The configuration for Diamond Head uses bathymetry parameters $A = 20$ m, $B = 400$ m, $C = 150$ km, $D = 25$ m with 301 grid points in the x-direction with a spacing of 0.5 km.

Appendix B. Numerical methods

B.1. Integration schemes

The partial differential equations describing advection of biological tracers are integrated using three iterations of a positive definite advection scheme (Smolarkiewicz, 1984). The ordinary differential equations describing biological transformations are integrated using an adaptive fifth order Cash-Karp Runge–Kutta method (Press et al., 1992) with an absolute tolerance of 10^{-9} mol N m^{-3} for N, P and Z and 10^{-9} for R_N and R_I.

B.2. Operator splitting

The numerical approximation of the advection (including sinking), diffusion, and the reaction of biological components by separate integrators and updating sequentially is called operator splitting. Operator splitting can be an accurate and efficient method of integrating advection–diffusion-reaction problems because the technique of solving each process can be tailored to its own particular numerical characteristics (Blom and Verwer, 2000). However, an error is introduced by splitting the numerical solution of these processes. This error can be significant if the model processes contain a large range of time scales. To test for such errors, two simple methods of operator splitting are employed, and the results compared. First the different integrations are undertaken sequentially [in the order advection (including sinking)–diffusion–biological reactions]. Secondly, the integrations are undertaken simultaneously (i.e. all changes were based on the original value). Throughout the model domain at all time steps the differences are small (less than 1% over a 2-min time step), suggesting that the sequential use of different integrating methods is sufficient for a simple plankton food web. For a stiffer set of ODEs, such as might be used for detailed chemical reactions, more elaborate control of splitting error is required (Blom and Verwer, 2000).

B.3. Conservation of mass requirements

Conservation of mass of the biogeochemical components is checked within each grid cell, and for the whole domain, at each time step using Eq. (8). The calculations proceed if each cell in the model domain conserves mass during the integration of the biological processes to within 10^{-9} mol N m^{-3}. The total volume of the model domain is 3.7×10^{10} m^3, and its total mass varies by less than 2 mol N throughout the simulations.

B.4. Advection–diffusion of plankton

The advection and diffusion of nonconservative tracers such as plankton require a spatial resolution that has a maximum value of:

$$\Delta x \approx \min\left[U/\gamma, \sqrt{D/\gamma}\right] \qquad (22)$$

where U is the typical advection velocity, γ is the exponential rate of change of the nonconservative tracer, and D is the horizontal diffusivity (Broström, 2002). If these criteria are exceeded, the plankton bloom can erroneously propagate at a different velocity to conservative tracers. In the model runs $\Delta x = 0.5$ km, and γ has a maximum for zooplankton of 4 day^{-1}. During model runs, the criteria are only violated when $U < 0.02$ m s^{-1} or $D < 0.0004$ m^2 s^{-1}. For these small values of U and D, advection and diffusion are not important terms.

Appendix C. Estimation of parameter values in the biomechanical model based on the Franks model with the Edwards et al. (2000a) parameter set

The equations describing biological processes in the Franks model have similar limits (such as maximum growth rate, zero growth rate, etc.) to the biomechanical model. The slope of the curve describing the biological processes at these limits can be used to match, as far as possible, the parameter sets of the Franks and biomechanical models. This matching involves determining what radii of phytoplankton and relative swimming speed between phytoplankton and zooplankton gives the same initial slope of DIN uptake and grazing in the biomechanical model, α_{BM}, as the slope found in the Franks model with the parameter values of Edwards et al. (2000a) study, α_E.

C.1. DIN uptake

Edwards et al. (2000a) uses a Monod growth curve to describe DIN uptake. The initial slope of uptake against DIN concentration in the Monod curve, α_E, in the unit system of this paper, is given by:

$$\alpha_E = \mu_P^{max}/k_s = 0.23 \text{ s}^{-1}\text{mol N}^{-1}\text{m}^3 \quad (23)$$

where $k_s = 0.1 \times 10^{-3}$ mol N m^{-3} is the half-saturation constant for DIN uptake and μ_P^{max} is 2.0 day^{-1} in the Edwards study. The equivalent initial slope of uptake against DIN concentration in the biomechanical model is given by $\alpha_{BM} = \psi D/m_{P,N} = 4\pi r_P D/m_{P,N}$ (Table 1). Using the relationship between $m_{P,N}$ and r_P from Table 1, the radius of phytoplankton, r_P, when α_E and α_{BM} are equal is given by:

$$r_P = \left(\frac{\mu_P^{max}/k_s}{4\pi D/(1.32(4\pi/3)^{0.758}16/106)}\right)^{(1/-1.274)} = 4.96 \approx 5 \text{ μm}. \quad (24)$$

C.2. Grazing

Edwards et al. (2000a) uses an Ivlev grazing function (Franks et al., 1986). The initial slope of grazing rate against phytoplankton concentration, not including the assimilation efficiency, is given by:

$$\alpha_E = \Lambda \mu_Z^{max} Z \quad (25)$$

where, with the appropriate change of units, $\Lambda = 300$ (mol N m^{-3})$^{-1}$ is the saturation constant of the Ivlev grazing function (Edwards et al., 2000a) and $\mu_Z^{max} = 4.0$ day^{-1} in the Edwards study. In the biomechanical model, three sources of relative motion between predator and prey are considered: diffusion, turbulent shear and relative velocity. For the purposes of determining a swimming velocity, only encounter rate due to relative velocity, ϕ_{vel}, will be considered. The equivalent initial slope of grazing rate against phytoplankton concentration in the biomechanical model is given by:

$$\alpha_{BM} = \frac{\phi_{vel} Z}{m_{P,N}}. \quad (26)$$

To solve for physical parameter values at which $\alpha_E = \alpha_{BM}$ requires using the biomechanical encounter rate formulation, $\phi_{vel} = 0.5\pi r_P^2 U$ (Table 1), where U is the relative velocity between the predator and prey, and $r_P = 5$ μm obtained from above. The relative encounter velocity, U, can be solved from Eqs. (25) and (26) as:

$$U = \frac{\Lambda \mu_Z^{max} 1.32(4\pi r_P^3/3)^{0.758}16/106}{0.5\pi r_P^2} = 180 \text{ μm s}^{-1}. \quad (27)$$

It is worth noting that a number of equation forms exist for encounter rates of predators and prey (Jackson, 1995). The curvilinear solution formulation has been used in this paper. The rectilinear form is

$\phi_{vel} = \pi(r_P + r_Z)^2 U$, where r_Z is the radius of the predator species. Using $r_Z = 50$ μm, the rectilinear solution requires a relative velocity, U, of 0.7 μm s^{-1}. The rectilinear solution, which does not include the effect of the predator cell on the flow path of the prey, predicts much higher encounter rates than the curvilinear solution, and therefore, for the same encounter rate, requires a much smaller relative velocity. The curvilinear solution appears to match the physical processes involved in cell encounters better than the rectilinear solution, and produces a more reasonable estimation of relative velocities. As a result, the curvilinear solution is the best choice for calculating ϕ.

A further calculation can be made to determine the level of dissipation of TKE that would result in a similar encounter rate of predator and prey as the Franks model grazing function with the Edwards microzooplankton parameter set. Taking $r_Z = 50$ μm, $\nu = 9 \times 10^{-7}$ m^2 s^{-1} and $\phi = 9.8(p^2/(1+2p)^2)(\epsilon/\upsilon)^{0.5}(r_P + r_Z)^3$, $p = r_P/r_Z$:

$$\epsilon = \left[1.32(4\pi r_P^3/3)^{0.758} \frac{16}{106} \Lambda \mu_Z^{max} \frac{(1+2p)^2}{9.8p^2} \times \frac{1}{(r_P + r_Z)^3} \right]^2 \nu = 3.7 \times 10^{-7}\ m^2\ s^{-3}. \quad (28)$$

This level of dissipation rate of TKE is only found in the surface and bottom boundary layers of the flow. The increased encounter in these regions can be best seen by the increasing grazing term in the top 10 m of the vertical profile of the phytoplankton terms for the stable mixed layer in Fig. 4.

References

Allen, J.S., Newberger, P.A., Federiuk, J., 1995. Upwelling circulation on the Oregon continental shelf: Part I. Response to idealized forcing. J. Phys. Oceanogr. 25, 1843–1866.

Baird, M.E., 2003. Numerical approximations of the mean absorption cross-section of a variety of randomly oriented microalgal shapes. J. Math. Biol. 47, 325–336.

Baird, M.E., Emsley, S.M., 1999. Towards a mechanistic model of plankton population dynamics. J. Plankton Res. 21, 85–126.

Baird, M.E., Emsley, S.M., McGlade, J.M., 2001. Modelling the interacting effects of nutrient uptake, light capture and temperature on phytoplankton growth. J. Plankton Res. 23, 829–840.

Baird, M.E., Walker, S.J., Wallace, B.B., Webster, I.T., Parslow, J.S., 2003. The use of mechanistic descriptions of algal growth and zooplankton grazing in an estuarine eutrophication model. Estuar. Coast. Shelf Sci. 56, 685–695.

Bax, N.J., Burford, M., Clementson, L., Davenport, S., 2001. Phytoplankton blooms and production sources on the southeast Australian continental shelf. Mar. Freshw. Res. 52, 451–462.

Blom, J.G., Verwer, J.G., 2000. A comparison of integration methods for atmospheric transport-chemistry problems. J. Comput. Appl. Math. 126, 381–396.

Blumberg, A.F., Mellor, G.L., 1987. A description of a three-dimensional coastal ocean circulation model. In: Heaps, N. (Ed.), Three-Dimensional Coastal Ocean Models. American Geophysical Union, Washington, DC, pp. 1–15.

Boyd, P.W., Watson, A.J., Law, C.S., et al., 2000. A meso-scale phytoplankton bloom in the polar Southern Ocean stimulated by iron fertilization. Nature 407, 695–702.

Brock, T.D., 1981. Calculating solar radiation for ecological studies. Ecol. Model. 14, 1–19.

Broström, G., 2002. On advection and diffusion of plankton in coarse resolution ocean models. J. Mar. Syst. 35, 99–110.

Caparroy, P., Thygesen, U.H., Visser, A., 2000. Modelling the attack success of planktonic predators: patterns and mechanisms of prey size selectivity. J. Plankton Res. 22, 1871–1900.

Craig, P.D., Banner, M.L., 1994. Modeling wave-enhanced turbulence in the ocean surface layer. J. Phys. Oceanogr. 24, 2546–2559.

Dela-Cruz, J., Ajani, P., Lee, R., Pritchard, T., Suthers, I., 2002. Temporal abundance patterns of the red tide dinoflagellate *Noctiluca scintillans* along the southeast coast of Australia. Mar. Ecol. Prog. Ser. 236, 75–88.

Dela-Cruz, J., Middleton, J.H., Suthers, I.M., 2003. Population growth and transport of the red tide dinoflagellate, *Noctiluca scintillans*, in the coastal waters off Sydney Australia, using cell diameter as a tracer. Limnol. Oceanogr. 48, 656–674.

Droop, M.R., 1983. 25 years of algal growth kinetics: a personal view. Bot. Mar. 26, 99–112.

Edwards, C.A., Batchelder, H.P., Powell, T.M., 2000a. Modeling microzooplankton and macrozooplankton dynamics within a coastal upwelling system. J. Plankton Res. 22, 1619–1648.

Edwards, C.A., Powell, T.M., Batchelder, H.P., 2000b. The stability of an NPZ model subject to realistic levels of vertical mixing. J. Mar. Res. 58, 37–69.

Elliott, J.A., Reynolds, C.S., Irish, T.E., 2000. The diversity and succession of phytoplankton communities in disturbance-free environments, using the model PROTECH. Arch. Hydrobiol. 149, 241–258.

Emsley, S.M., 2000. PECOS Towards an Object-oriented Virtual Ecology of Plankton Population Dynamics. PhD thesis, University of Warwick.

Finkel, Z.V., 2001. Light absorption and size scaling of light-limited metabolism in marine diatoms. Limnol. Oceanogr. 46, 86–94.

Finkel, Z.V., Irwin, A.J., 2000. Modeling size-dependent photosynthesis: light absorption and the allometric rule. J. Theor. Biol. 204, 361–369.

Franks, P.J.S., Chen, C., 2000. A 3-D prognostic numerical model

study of the Georges Bank ecosystem: Part II. Biological-physical model. Deep-Sea Res., Part 2, Top. Stud. Oceanogr. 48, 457–482.

Franks, P.J.S., Wroblewski, J.S., Flierl, G.R., 1986. Behaviour of a simple plankton model with food-level acclimation by herbivores. Mar. Biol. 91, 121–129.

Gillooly, J.F., 2000. Effect of body size and temperature on generation time in zooplankton. J. Plankton Res. 22, 241–251.

Hansen, B., Bjornsen, P.K., Hansen, P.J., 1994. The size ratio between planktonic predators and prey. Limnol. Oceanogr. 39, 395–403.

Hansen, P.J., Bjornsen, P.K., Hansen, B.W., 1997. Zooplankton grazing and growth: scaling within the 2–2,000 μm body size range. Limnol. Oceanogr. 42, 687–704.

Hein, M., Pedersen, M.F., Sand-Jensen, K., 1995. Size-dependent nitrogen uptake in micro- and macroalgae. Mar. Ecol. Prog. Ser. 118, 247–253.

Hofmann, M., Wolf-Gladrow, D.A., Takahashi, T., Sutherland, S.C., Six, K.D., Maier-Reimer, E., 2000. Stable carbon isotope distribution of particulate organic matter in the ocean: a model study. Mar. Chem. 72, 131–150.

Jackson, G.A., 1995. Coagulation of marine algae. In: Huang, C.P., O'Melia, C.R., Morgan, J.J. (Eds.), Aquatic Chemistry: Interfacial and Interspecies Processes. American Chemical Society, Washington, DC, pp. 203–217.

Kiørboe, T., 1993. Turbulence, phytoplankton cell size, and the structure of pelagic food webs. Adv. Mar. Biol. 29, 1–72.

Kirk, J.T.O., 1994. Light and Photosynthesis in Aquatic Ecosystems, 2nd edition Cambridge Univ. Press, Cambridge.

Li, Y., Gregory, S., 1974. Diffusion of ions in seawater and in deep-sea sediments. Geochim. Cosmochim. Acta 38, 703–714.

Marchesiello, P., Gibbs, M., Middleton, J.H., 2000. Simulations of coastal upwelling on the Sydney continental shelf. Mar. Freshw. Res. 51, 577–588.

Mellor, G.L., Yamada, T., 1982. Development of a turbulent closure model for geophysical fluid problems. Rev. Geophys. Space Phys. 20, 851–875.

Oke, P.R., Middleton, J.H., 2001. Nutrient enrichment off Port Stephens: the role of the East Australian Current. Cont. Shelf Res. 21, 587–606.

Press, W.H., Flannery, B.P., Teukolsky, S.A., Vetterling, W.T., 1992. Numerical Recipes in Fortran 77: The Art of Scientific Programming, 2nd edition Cambridge Univ. Press, Cambridge.

Redfield, A.C., Ketchum, B.H., Richards, F.A., 1963. The influence of organisms on the composition of seawater. In: Hill, J.M.N. (Ed.), The Sea—The Composition of Sea-Water and Comparative and Descriptive Oceanography, vol. 2, 2nd edition. Wiley, New York, pp. 26–77.

Reynolds, C.S., 1984. The Ecology of Freshwater Phytoplankton. Cambridge Univ. Press, Cambridge.

Reynolds, C.S., 1989. Physical determinants of phytoplankton succession. In: Sommer, U. (Ed.), Plankton Ecology. Springer-Verlag, Berlin, pp. 9–51.

Ridgway, K.R., Dunn, J.R., Wilkin, J.L., 2002. Ocean interpolation by four-dimensional least squares—application to the waters around Australia. J. Atmos. Ocean. Technol. 19, 1357–1375.

Rochford, D.J., 1972. Nutrient enrichment of east Australian coastal waters: I. Evans Head upwelling. Tech. rep., Division of Fisheries and Oceanography, CSIRO, Australia.

Roughan, M., Middleton, J.H., 2002. A comparison of observed upwelling mechanisms off the east coast of Australia. Cont. Shelf Res. 22, 2551–2572.

Sharples, J., Tett, P., 1994. Modelling the effect of physical variability on the midwater chlorophyll maximum. J. Mar. Res. 52, 219–238.

Sheldon, R.W., Prakash, A., Sutcliffe, W.H., 1972. The size distribution of particles in the ocean. Limnol. Oceanogr. 17, 327–340.

Smagorinsky, J., 1963. General circulation experiments with primitive equations. Mon. Weather Rev. 91, 99–164.

Smolarkiewicz, P.K., 1984. A fully multidimensional positive definite advection transport algorithm with small implicit diffusion. J. Comput. Phys. 54, 325–362.

Sommer, U., 1988. Some size relationships in phytoflagellate motility. Hydrobiologia 161, 125–131.

Spitz, Y., Newberger, P., Allen, J., 2003. Ecosystem response to upwelling off the Oregon coast: behavior of three nitrogen-based models. J. Geophys. Res. 108 (C3), 3062–3084.

Strathmann, R.R., 1967. Estimating the organic carbon content of phytoplankton from cell volume or plasma volume. Limnol. Oceanogr. 12, 411–418.

Tang, E.P.Y., 1995. The allometry of algal growth rates. J. Plankton Res. 17, 1325–1335.

Tang, E.P.Y., Peters, R.H., 1995. The allometry of algal respiration. J. Plankton Res. 17, 303–315.

Wijesekera, H.W., Allen, J.S., Newberger, P.A., 2003. Modeling study of turbulent mixing over the continental shelf: comparison of turbulent closure schemes. J. Geophys. Res. 108 (C3), 3103.

Wolf-Gladrow, D., Riebesell, U., 1997. Diffusion and reactions in the vicinity of plankton: a refined model for inorganic carbon transport. Mar. Chem. 59, 17–34.